Journal of Materials Chemistry A

PAPER

View Article Online
View Journal | View Issue

Cite this: J. Mater. Chem. A, 2016, 4, 4893

A synergistic effect between layer surface configurations and K ions of potassium vanadate nanowires for enhanced energy storage performance†

Jiashen Meng,‡ Ziang Liu,‡ Chaojiang Niu,‡ Xiaoming Xu, Xiong Liu, Guobin Zhang, Xuanpeng Wang, Meng Huang, Yang Yu and Liqiang Mai*

Layered metal vanadates, especially alkali metal vanadates, have been extensively studied in energy storage. Generally, vanadates exhibit more stable electrochemical performance than pristine vanadium oxides, and different vanadates also vary in the performance. However, the detailed mechanisms of the variation in the performance of vanadates and vanadium oxides are poorly explored. Here we choose and construct three typical layered vanadium-based nanowires (V_2O_5, KV_3O_8 and $K_{0.25}V_2O_5$), and investigate the origin of the enhanced electrochemical performance of the potassium vanadates compared to V_2O_5, based on crystal structure analysis, electrochemical tests, *ex situ* ICP measurements and *in situ* XRD detections. We demonstrate a synergistic effect between layer surface configurations and K ions of potassium vanadate nanowires, which leads to the great improvement in electrochemical stability of $K_{0.25}V_2O_5$. The layer surface configuration of $K_{0.25}V_2O_5$ only consists of single-connected oxygen atoms, which provides strong interaction with the K ions. And the stabilized K ions act as "pillars" between interlayers to protect the layered structures from collapse in the charge/discharge process. This work provides a further insight into alkali metal vanadates, and benefits the design of ideal electrode materials in the energy storage field.

Received 20th January 2016
Accepted 1st March 2016

DOI: 10.1039/c6ta00556j

www.rsc.org/MaterialsA

Introduction

With the rapid development of portable electronics, electric vehicles (EV) and hybrid electric vehicles (HEV), rechargeable batteries are undoubtedly one of the best candidates among various energy storage devices for chemically storing energy.[1] Until now, intensive efforts have been focused on developing rechargeable batteries with high energy density, high power density, high cycling stability and low cost.[2–5] Compared with anode materials, cathode materials become a big bottleneck of battery breakthroughs due to their relatively low capacities.[6–9] Therefore, developing battery cathode materials with high capacity and low cost has been a crucial issue for both the fundamental study and practical application.[10–14]

Generally, cathode materials can be categorized into four main groups according to their crystal structures: layer type, spinel type, olivine type, and NASICON type.[15–21] Among them, layered oxides are one of the most extensively studied topics in lithium and sodium ion batteries. To our knowledge, well-developed and commercial layered oxides, such as $LiCoO_2$, $LiNi_{1/3}Co_{1/3}Mn_{1/3}O_2$, *etc.*, have been widely investigated and applied for lithium-ion batteries.[16] Moreover, for sodium ion batteries, the common Na_xMeO_2 layered oxides (Me = 3d transition metals), are built up of a sheet of edge-sharing [MeO_6] octahedra.[4] For example, Komaba *et al.* reported P2-$Na_{2/3}Fe_{1/2}Mn_{1/2}O_2$ made from earth-abundant elements, that delivers a reversible capacity of 190 mA h g^{-1} in sodium cells.[20] Therefore, intensive efforts have been dedicated to developing layered oxides with different stacked units in period, varying in their electrochemical performance for lithium and sodium ion batteries.[22–24]

Due to their abundant resources, easy preparation, stable thermodynamic properties and high theoretical capacities, vanadates, such as LiV_3O_8, $Na_{1.25}V_3O_8$, NaV_6O_{15}, $K_{0.25}V_2O_5$, *etc.*, have been remarkably attractive candidates among layered oxides as lithium and sodium ion battery cathodes.[25–31] Liu *et al.* fabricated single crystalline NaV_6O_{15} nanorods *via* a hydrothermal route, which possessed enhanced electrochemical behaviour as a cathode in rechargeable lithium ion batteries.[26] Due to their structural stability and increased interlayer spaces, these vanadates also exhibit excellent sodium storage properties. Dong *et al.* reported hierarchical zigzag $Na_{1.25}V_3O_8$

State Key Laboratory of Advanced Technology for Materials Synthesis and Processing, Wuhan University of Technology, Wuhan 430070, China. E-mail: mlq518@whut.edu.cn

† Electronic supplementary information (ESI) available: Crystallographic parameters, CV curves, AC impedance plots, XRD pattern and SEM image of $H_2V_3O_8$ nanowires, and ICP test results. See DOI: 10.1039/c6ta00556j

‡ These authors contributed equally to this work.

nanowires, showing superior cycling stability and high rate capacities as a sodium ion battery cathode.[32] In our previous report, we investigated isostructural alkali metal vanadates (Li, Na, and K-V_6O_{15}) as lithium ion battery cathodes.[33] It was found that K-V_6O_{15} exhibits better electrochemical performance than V_2O_5, and also shows better rate capability and cycling stability than Li-V_6O_{15} and Na-V_6O_{15}. Based on experimental characterization and theoretical calculations, a synergistic effect between the layer surface structure and different alkali metal ions was proposed.[32]

To further demonstrate the synergistic effect and explore the enhanced mechanism of electrochemical performance, this work focuses on vanadates with different layer surface configurations and the same alkaline metal ions. Here we purposefully choose and construct three typical layered vanadium-based nanowires (V_2O_5, KV_3O_8 and $K_{0.25}V_2O_5$), and investigate the origin of the enhanced electrochemical performance of the potassium vanadates. The layer surface configurations of the potassium vanadates play a key role in their electrochemical stability. The K ions between interlayers in $K_{0.25}V_2O_5$ are more stable than those in KV_3O_8 due to the stronger interaction between K ions and single-connected oxygen atoms on the layer surface. And the stabilized K ions act as "pillars" between interlayers to protect the layered structures from collapse during the charge/discharge processes. Therefore, the synergistic effect between layer surface configurations and K ions is of great importance for the performance of potassium vanadate nanowires.

Experimental

Preparation of V_2O_5 nanowires

First, single crystalline $H_2V_3O_8$ nanowires were synthesized by a hydrothermal method according to our previous work.[33] Briefly, 1.3 mmol as-prepared V_2O_5 sol, 3.6 mL aniline, and 0.04 g poly(ethylene glycol) (PEG-4000) were mixed by stirring and then transferred into a Teflon-lined stainless steel autoclave and kept at 180 °C for 48 h. The products were collected and washed repeatedly with deionized water and ethanol, and finally dried at 80 °C for 12 h in air to obtain $H_2V_3O_8$ nanowires. Second, after the $H_2V_3O_8$ nanowires were sintered at 400 °C for 2 h, V_2O_5 nanowires were obtained.

Preparation of KV_3O_8 nanowires

$H_2V_3O_8$ nanowires and KOH were mixed in alcohol and stirred for 6 h. Then after drying at 70 °C for 6 h, the mixture was annealed at 400 °C for 10 h in air to obtain a reddish brown powder. Thus KV_3O_8 nanowires were obtained.

Preparation of $K_{0.25}V_2O_5$ nanowires

In a typical synthesis, 0.100 g of polyethyleneglycol (PEG-4000), 0.1818 g of V_2O_5 powder, and 0.35 mL of KOH (1 mol L^{-1}) were added in 30 mL of deionized water under vigorous magnetic stirring at room temperature for 2 h. Then, the mixture was transferred to a 50 mL autoclave and maintained in an oven at 180 °C for 48 h. The products were collected and washed repeatedly with deionized water and ethanol, and finally dried at 80 °C for 12 h in air. Then, the dried sample was annealed at 525 °C for 5 h in air to obtain $K_{0.25}V_2O_5$ nanowires.

Materials characterization

The crystallographic information of the final products was obtained using a Bruker D8 Discover X-ray diffractometer equipped with a Cu Kα radiation source; the samples were scanned over the 2θ range from 10° to 60° at room temperature. The SEM images were collected using a JEOL-7100F scanning electron microscope, and the TEM images were collected using a JEM-2100F transmission electron microscope. Inductively coupled plasma (ICP) tests were carried out using an Optima 4300DV.

Electrochemical characterization

2016 coin cells were assembled in a glovebox filled with pure argon. The cathode was composed of a ground mixture of 70% active material, 20% acetylene black and 10% poly(tetrafluoroethylene) (PTFE). After coating onto aluminum foil, the electrode film was uniformly cut into about 0.5 cm^2 (area) round slices, weighing a total of about 1.2 mg; the corresponding areal mass loading was 2.4 mg cm^{-2}. For lithium ion batteries, lithium foil was used as the anode and a solution of $LiPF_6$ (1 M) in EC/DEC (1 : 1 vol/vol) was used as the electrolyte. For sodium ion batteries, sodium discs were used as the anode and 1 M $NaClO_4$ in a mixture of ethylene carbon/dimethyl carbonate (1 : 1 w/w) with 2.0 wt% propylene carbonate (electrolyte additive) was used as the electrolyte. Galvanostatic charge/discharge measurements were performed using a multichannel battery testing system (LAND CT2001A). Cyclic voltammograms (CV) and electrochemical impedance spectra (EIS) were collected at room temperature using an Autolab potentiostat/galvanostat. For *in situ* XRD measurements, the electrode was placed right behind an X-ray-transparent beryllium window which also acts as a current collector. The *in situ* XRD signals were collected using a planar detector in a still mode during the discharge–charge process, and each pattern took 2 min to acquire.

Results and discussion

Morphology and structural characterization

First, the crystal structures of V_2O_5, KV_3O_8 and $K_{0.25}V_2O_5$ are illustrated (Fig. 1). V_2O_5 is a typical layered structure with a layer spacing of 4.36 Å. In comparison, KV_3O_8 and $K_{0.25}V_2O_5$ exhibit

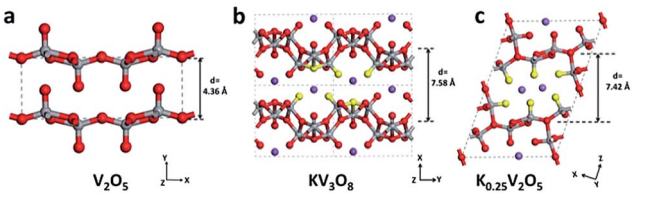

Fig. 1 Illustrations of the crystal structures of V_2O_5 (a), KV_3O_8 (b) and $K_{0.25}V_2O_5$ (c), respectively. The red and yellow balls represent O atoms; grey and purple balls represent V atoms and K ions, respectively.

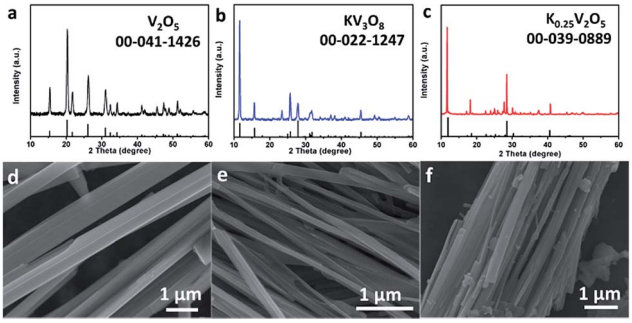

Fig. 2 XRD patterns and SEM images of V_2O_5 (a and d), KV_3O_8 (b and e) and $K_{0.25}V_2O_5$ (c and f) nanowires.

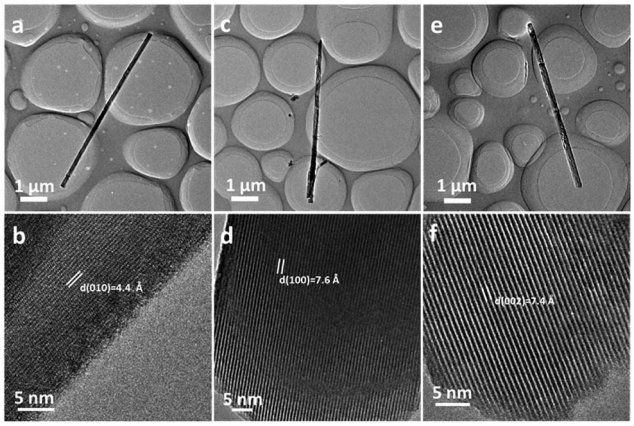

Fig. 3 TEM images of V_2O_5 (a and b), KV_3O_8 (c and d) and $K_{0.25}V_2O_5$ (e and f) nanowires, respectively.

different layered structures with K ions distributed in the interlayers (Table S1†). And the layer spacing expands to 7.58 Å for KV_3O_8 and 7.42 Å for $K_{0.25}V_2O_5$, respectively. Notably, these two potassium vanadates have different layer surface configurations (as the yellow balls displayed in Fig. 1). The layer surface of KV_3O_8 is composed of single-connected and tri-connected oxygen atoms. However, all the oxygen atoms on the layer surface of $K_{0.25}V_2O_5$ are single-connected, which can bond and provide strong interaction with K ions.

V_2O_5, KV_3O_8 and $K_{0.25}V_2O_5$ nanowires are synthesized *via* a facile hydrothermal method and subsequent heat treatment (Fig. S1†).[34] Their XRD patterns show no impurities (Fig. 1a–c). V_2O_5 nanowires are orthorhombic phase (JCPDS no. 00-041-1426), while both KV_3O_8 and $K_{0.25}V_2O_5$ nanowires are both monoclinic phases (JCPDS no. 00-022-1247; JCPDS no. 00-039-0889). As shown in the SEM images, these nanowires display an average diameter of 100–300 nm and a smooth surface (Fig. 2d–f). As shown in TEM images, the length/diameter ratios are more than 50 (Fig. 3). From HRTEM images, the interlayer spacings of V_2O_5, KV_3O_8 and $K_{0.25}V_2O_5$ nanowires are calculated to be 4.4 Å, 7.6 Å and 7.4 Å, well consistent with the corresponding lattice planes of (010), (100) and (002), respectively. These layers are parallel to the nanowires.

Electrochemical performance

To compare the electrochemical performances of the V_2O_5, KV_3O_8 and $K_{0.25}V_2O_5$ nanowires, CV measurements were performed to explore the phase transformation at potentials ranging from 1.5 to 4.0 V at a scan rate of 0.2 mV s^{-1} (Fig. S2†). As shown in Fig. S2a,† four sharp reduction peaks of V_2O_5 nanowires occur at potentials of 3.35, 3.14, 2.12, and 1.91 V, during the first discharge cycle. These sharp peaks correspond to the phase transformations from V_2O_5 to ε-$Li_{0.5}V_2O_5$, δ-LiV_2O_5, γ-$Li_2V_2O_5$ and ω-$Li_3V_2O_5$.[35–37] However, in the subsequent charge process, two broad oxidization peaks at 2.45 and 2.68 V show obvious irreversible behaviour. The charge/discharge curves of V_2O_5 nanowires are characterized at a current density of 100 mA g^{-1} (Fig. S2d†). After the first discharge process, the subsequent charge/discharge curves have no obvious voltage platforms, which correspond to the broad peaks of CV curves. In a previous report, the irreversible behaviour occurred in V_2O_5, which was due to the irreversible formation of ω-$Li_3V_2O_5$ at a voltage lower than 1.9 V.[38] The CV curve of KV_3O_8 nanowires has a pair of redox peaks, namely 2.33 V and 2.84 V (Fig. S2b†). The corresponding charge–discharge curves of KV_3O_8 nanowires show that the first and second cycles are similar except for the small capacity fading (Fig. S2e†). Compared with V_2O_5 and KV_3O_8 nanowires, $K_{0.25}V_2O_5$ nanowires exhibit better reversible behaviour and lower overpotential as observed from CV and charge/discharge curves (Fig. S2c and f†). Notably, the cathodic peaks below 1.9 V, corresponding to the irreversible phase transition of V_2O_5, disappeared in KV_3O_8 and $K_{0.25}V_2O_5$ nanowires.[38] To study the theoretical capacities of V_2O_5, KV_3O_8 and $K_{0.25}V_2O_5$ nanowires, the galvanostatic intermittent titration technique (GITT) test is conducted (Fig. S3†). The V_2O_5 nanowires show a theoretical discharge capacity of 412 mA h g^{-1} (nearly 3 Li insertions per unit formula), which is consistent with those results previously reported.[36–38] The KV_3O_8 and $K_{0.25}V_2O_5$ nanowires show a theoretical discharge capacity of 327 and 341 mA h g^{-1}, respectively.

Meanwhile, more electrochemical measurements of V_2O_5, KV_3O_8 and $K_{0.25}V_2O_5$ nanowires were performed for lithium ion batteries. When tested at a current density of 100 mA g^{-1}, the initial discharge capacities of V_2O_5, KV_3O_8 and $K_{0.25}V_2O_5$ nanowires were 353, 301, and 292 mA h g^{-1}, respectively. The initial discharge capacities of KV_3O_8 and $K_{0.25}V_2O_5$ nanowires were lower than that of V_2O_5 nanowires due to the partial occupation of K ions in the available Li ion intercalation sites. The corresponding first coulombic efficiencies of V_2O_5, KV_3O_8 and $K_{0.25}V_2O_5$ nanowires in lithium ion batteries were 93%, 95%, and nearly 100%, respectively. Moreover, 20%, 55% and 92% (*i.e.*, 71, 165 and 270 mA h g^{-1}) were retained after 100 cycles at 100 mA g^{-1} (Fig. 4a). The rate performance was measured at various current densities of 100, 200, 300, 500, and 1000 mA g^{-1} (Fig. 4b). As shown in Fig. 4b, the $K_{0.25}V_2O_5$ nanowires possess excellent rate performance. The average discharge capacities of 286, 273, 252, 241, and 187 mA h g^{-1}, respectively, were obtained at these rates. The corresponding charge/discharge curves at different current densities are shown in Fig. S4.† When the current density was back to 100 mA g^{-1},

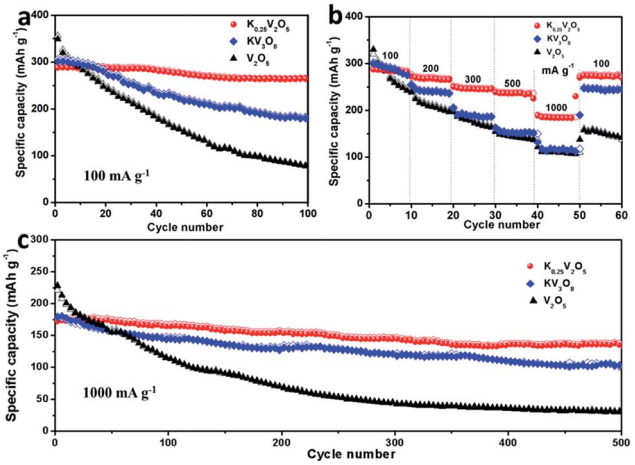

Fig. 4 Electrochemical performances of V_2O_5, KV_3O_8 and $K_{0.25}V_2O_5$ nanowires in lithium ion batteries. (a) Cycling performance tested at a low current density of 100 mA g^{-1}. (b) Rate performance tested at current densities of 100, 200, 300, 500 and 1000 mA g^{-1}. (c) Cycling performance tested at a high current density of 1000 mA g^{-1}.

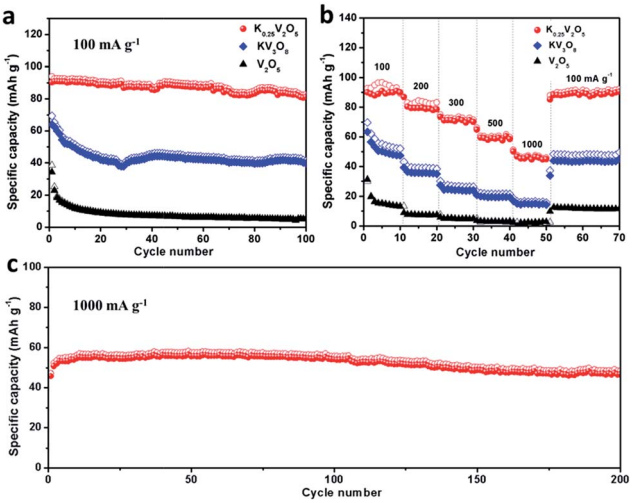

Fig. 5 Electrochemical performance of V_2O_5, KV_3O_8 and $K_{0.25}V_2O_5$ nanowires in sodium ion batteries. (a) Cycling performance tested at a low current density of 100 mA g^{-1}. (b) Rate performance tested at current densities of 100, 200, 300, 500 and 1000 mA g^{-1}. (c) Cycling performance of $K_{0.25}V_2O_5$ nanowires tested at a high current density of 1000 mA g^{-1}.

the average discharge capacity was 271 mA h g^{-1} with a capacity recovery of 95%, superior to that of V_2O_5 and KV_3O_8 nanowires (*i.e.*, 55% and 80%, respectively). In addition, when tested at a high current density of 1000 mA g^{-1}, the first discharge capacities of V_2O_5, KV_3O_8 and $K_{0.25}V_2O_5$ nanowires were 225, 178 and 172 mA h g^{-1}, with the capacity retention of 14%, 62% and 83% after 500 cycles, respectively (Fig. 4c). EIS measurements were carried out (Fig. S5†). The charge transfer resistance (R_{ct}) of $K_{0.25}V_2O_5$ nanowires is 124 Ω, which is lower than those of V_2O_5 and KV_3O_8 nanowires (252 Ω and 170 Ω, respectively), showing higher efficient electron/ion transport. All results demonstrate that potassium vanadate nanowires exhibit better electrochemical performance than V_2O_5 when used as lithium ion battery cathodes. Meanwhile, $K_{0.25}V_2O_5$ nanowires show better electrochemical stability than the KV_3O_8 nanowires.

To further confirm the above observed law, V_2O_5, KV_3O_8 and $K_{0.25}V_2O_5$ nanowires were also characterized for sodium ion batteries. Initially, V_2O_5, KV_3O_8 and $K_{0.25}V_2O_5$ nanowires were tested at a current density of 100 mA g^{-1} (Fig. 5a). The first discharge capacities were 35, 68 and 90 mA h g^{-1}. After 100 cycles, the capacity retentions were 24%, 59% and 90%, respectively. The corresponding typical charge–discharge profiles of V_2O_5, KV_3O_8 and $K_{0.25}V_2O_5$ nanowires are shown in Fig. S6.† As previously reported, orthorhombic V_2O_5 for sodium ion battery application experienced deterioration and eventual loss of crystallinity after cycling, leading to fast capacity fading.[39] Subsequently, the rate performance was determined at rates of 100, 200, 300, 500, and 1000 mA g^{-1} (Fig. 5b). When the current density was returned to 100 mA g^{-1}, the capacity recovery of $K_{0.25}V_2O_5$ nanowires was nearly 100% and the 70th-cycle discharge capacity reached 90 mA h g^{-1}, showing great structural stability and excellent reversibility. In particular, an 88% retention of the top discharge capacity after 200 cycles at a high current density of 1000 mA g^{-1} also testified the excellent cycling performance of $K_{0.25}V_2O_5$ nanowires (Fig. 5c).

Synergistic effect in potassium vanadate nanowires

To reveal the enhanced mechanism in the electrochemical performance of potassium vanadate, $K_{0.25}V_2O_5$ and V_2O_5 nanowires were characterized by time-resolved *in situ* XRD during lithium ion insertion and extraction. A clear variation in the appropriate selective regions of $K_{0.25}V_2O_5$ and V_2O_5 nanowires was observed during the original cycles of galvanostatic charge and discharge at potentials ranging from 1.5 to 4.0 V and a current density of 150 mA g^{-1} (Fig. 6). In Fig. 6a, the (002), (104) and (30−4) reflection peaks of $K_{0.25}V_2O_5$ nanowires shift repeatedly during the galvanostatic charge and discharge process. Generally speaking, lithium/sodium ions insert into the cathodes during the discharge process and increase the interlayer spacings along with main peaks shifting toward low angles. Particularly, when the lithium ions insert into the $K_{0.25}V_2O_5$, these peaks shift toward high angles. The lithium ion insertion process can be expressed as:

$$K_{0.25}V_2O_5 + xLi^+ + xe^- \rightarrow Li_xK_{0.25}V_2O_5.$$[26]

The interlayer spacing of (002) changes from 7.42 Å to 7.14 Å based on the Bragg equation. The crystal structure of $K_{0.25}V_2O_5$ consists of VO_5 pyramids and VO_6 octahedra to form $(V_2O_5)_x$ frameworks. The inserted lithium ions may form covalent bonds with the oxygen atoms in the $(V_2O_5)_x$ frameworks and reduce the average $(V_2O_5)_x$ anion radius. The changing amplitudes of the main peaks are smaller than that of V_2O_5 nanowires. It indicates that K ions can act as "pillars" in between V–O layers to maintain the structural stability, increase parallel spacing and avoid the irreversible reaction. On the other hand, the selective (001), (201) and (110) reflection peaks of V_2O_5 nanowires change during the galvanostatic charge and discharge processes (Fig. 6b). It is

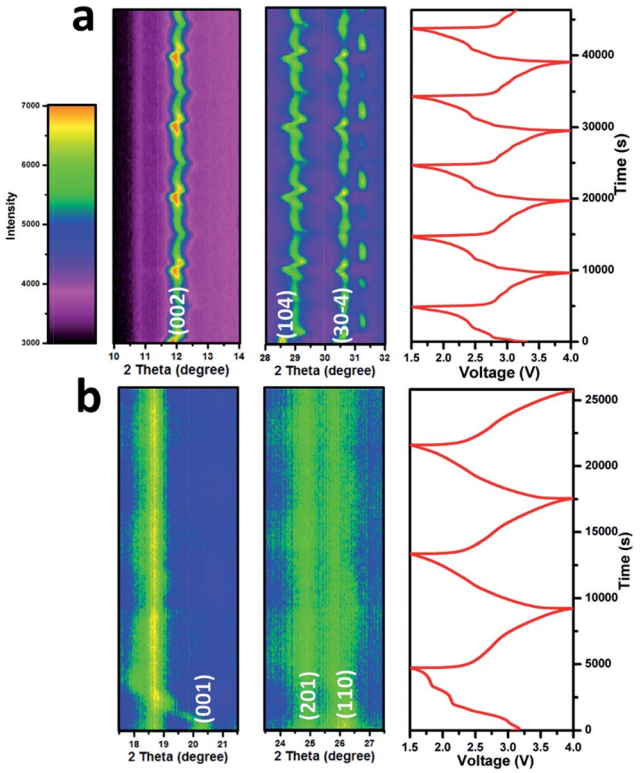

Fig. 6 *In situ* X-ray diffraction patterns of $K_{0.25}V_2O_5$ nanowires (a) and V_2O_5 nanowires (b) during galvanostatic charge and discharge at 150 mA g^{-1} in lithium ion batteries. The horizontal axis represents the selected 2θ regions, and time is on the vertical axis. The diffraction intensity is colour coded with the scale bar shown on the left. The corresponding voltage curve is plotted to the right.

obvious that the main diffraction peak of (001) disappears after the first discharge process, showing its irreversibility. At first, the length of the *c*-axis in the V_2O_5 crystal cell increases in the shallow discharge process and then the structural integrity is destroyed in the deep discharge process. Combined with CV curves, the phases evolve from V_2O_5 to ε-$Li_{0.5}V_2O_5$, δ-LiV_2O_5, γ-$Li_2V_2O_5$ and ω-$Li_3V_2O_5$. As previously reported, irreversible ω-$Li_3V_2O_5$ was formed followed by the wide solid solution process.[38]

To reveal the reason why $K_{0.25}V_2O_5$ nanowires show better electrochemical stability than KV_3O_8 nanowires, time-resolved *in situ* XRD results were first compared. In Fig. S7,† the (100) reflection of KV_3O_8 nanowires shifts repeatedly for the initial charge and discharge process. However, compared with the stable peaks of $K_{0.25}V_2O_5$, the (100) peak position of KV_3O_8 in the charge state shifts to a high angle gradually after several cycles, and the peak becomes wider and intensity also decreases, which indicates the collapse and amorphization of the KV_3O_8 layered structure in the lithium insertion–extraction process. In addition, ICP tests were carried out to directly detect the change in the K ion amount in potassium vanadate nanowire cathodes. After 100 cycles at 100 mA g^{-1}, the coin cells were disassembled and the $K_{0.25}V_2O_5$ and KV_3O_8 nanowire cathodes were washed with pure alcohol and deionized water. The molar ratios of K : V in $K_{0.25}V_2O_5$ nanowire cathodes change from 0.252 : 2 to 0.241 : 2, corresponding to the K loss ratio of 4.4%. However, in KV_3O_8 nanowires, the molar ratios change from 1.013 : 3 to 0.792 : 3, and the K loss ratio is 21.8% (Table S2†), indicating that the K ions in $K_{0.25}V_2O_5$ are more stable than in KV_3O_8. Therefore, the more stabilized K ions in the interlayers lead to better electrochemical stability.

On the basis of the crystal structure analysis, electrochemical tests, *in situ* XRD detections and *ex situ* ICP measurements, the lithium/sodium intercalation/deintercalation processes of V_2O_5, KV_3O_8 and $K_{0.25}V_2O_5$ can be illustrated as shown in Fig. 7.[40] For pristine V_2O_5 nanowires (Fig. 7a), owing to the lack of ion pillars, the intercalation of lithium/sodium ions into the interlayer sites will lead to an irreversible structural transformation and severe structural degradation in the initial cycles, thus resulting in fast capacity loss. For potassium vanadate nanowires, the K ions between interlayers can bond with the single-connected oxygen atoms and act as "pillars" to protect the layered structures from collapse. However, for KV_3O_8, there are tri-connected oxygen atoms existing on the layer surface, which cannot provide strong interaction with the K ions, causing the instability of K ions in the interlayers. After several charge–discharge cycles, partial K ions were extracted from the crystal structure (as demonstrated by the ICP measurements) which leads to the weakening of the pillar effect. And then structural degradation occurs (as demonstrated by the *in situ* XRD results), which results in capacity fading. For $K_{0.25}V_2O_5$ nanowires (Fig. 7c), the layer surface consists of only single-connected oxygen atoms, which can form strong interaction with K ions, and the firmly fixed K ions in the interlayers act as "pillars" to maintain the structural integrity, leading to excellent cycling performance during the charge/discharge process.

In brief, the superior electrochemical stability of $K_{0.25}V_2O_5$ is attributed to the synergistic effect between its layer surface configuration and the K ions in the interlayers: the layer surface consisting of single-connected oxygen atoms provides strong interaction with the K ions, and the stable K ions in the

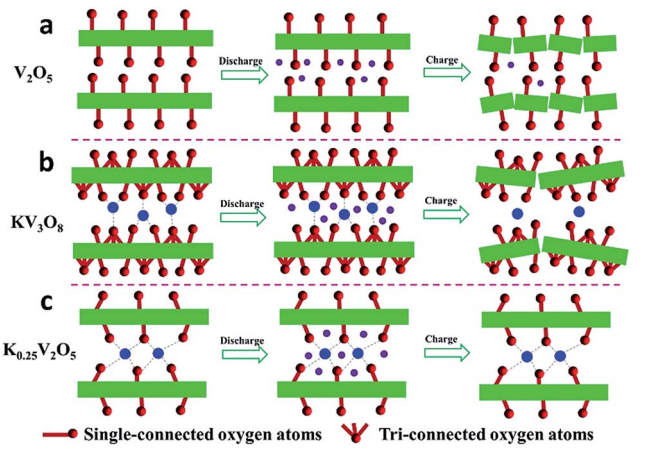

Fig. 7 Schematic illustrations of lithium/sodium intercalation/deintercalation processes of V_2O_5 (a), KV_3O_8 (b) and $K_{0.25}V_2O_5$ (c) for the initial cycles, respectively. The red balls, purple balls, and blue balls represent the O atoms, Li/Na ions and K ions, respectively.

interlayers act as "pillars" to prevent the structure from degradation, leading to outstanding electrochemical performance.

Conclusions

We purposefully prepared V_2O_5, KV_3O_8 and $K_{0.25}V_2O_5$ nanowires *via* a facile hydrothermal method and subsequent heat treatment. Compared with pristine V_2O_5, the potassium vanadate nanowires exhibit great improvement in electrochemical performance. Moreover, $K_{0.25}V_2O_5$ nanowires display better electrochemical stability than KV_3O_8 nanowires. Based on the crystal structure analysis, electrochemical tests, *in situ* XRD detections and *ex situ* ICP measurements, we conclude that the synergistic effect between layer surface configurations and the K ions results in $K_{0.25}V_2O_5$ nanowires with outstanding electrochemical stability. Namely, the single-connected oxygen atoms on the layer surface provide strong interaction with the K ions, and the stable K ions in the interlayers act as "pillars" to prevent the structure from degradation, leading to better electrochemical performance. This work provides a further insight into the structure–property correlation of alkali metal vanadates when used as energy storage materials, and provides a better direction for the design of ideal electrode materials in the energy storage field.

Acknowledgements

This work was supported by the National Basic Research Program of China (2013CB934103 and 2012CB933003), the International Science & Technology Cooperation Program of China (2013DFA50840), the National Natural Science Foundation of China (51521001 and 51272197), the National Natural Science Fund for Distinguished Young Scholars (51425204), the Hubei Provincial Natural Science Fund for Distinguished Young Scholars (2014CFA035), and the Fundamental Research Funds for the Central Universities (WUT: 2015-III-021, 2015-III-032, 2015-PY-2). We thank Prof. D. Y. Zhao of Fudan University and Prof. J. Liu of Pacific Northwest National Laboratory for useful discussions and assistance with the manuscript.

Notes and references

1 Z. G. Yang, J. L. Zhang, M. C. Kintner-Meyer, X. C. Lu, D. Choi, J. P. Lemmon and J. Liu, *Chem. Rev.*, 2011, **111**, 3577–3613.
2 M. Armand and J.-M. Tarascon, *Nature*, 2008, **451**, 652–657.
3 L. Q. Mai, X. C. Tian, X. Xu, L. Chang and L. Xu, *Chem. Rev.*, 2014, **114**, 11828–11862.
4 N. Yabuuchi, K. Kubota, M. Dahbi and S. Komaba, *Chem. Rev.*, 2014, **114**, 11636–11682.
5 V. Palomares, M. Casas-Cabanas, E. Castillo-Martínez, M. H. Han and T. Rojo, *Energy Environ. Sci.*, 2013, **6**, 2312–2337.
6 W. Luo, S. Lorger, B. Wang, C. Bommier and X. L. Ji, *Chem. Commun.*, 2014, **50**, 5435–5437.
7 Z. Y. Wang, L. Zhou and X. W. David Lou, *Adv. Mater.*, 2012, **24**, 1903–1911.
8 C. Yuan, H. B. Wu, Y. Xie and X. W. Lou, *Angew. Chem., Int. Ed.*, 2014, **53**, 1488–1504.
9 D. R. Rolison, J. W. Long, J. C. Lytle, A. E. Fischer, C. P. Rhodes, T. M. McEvoy, M. E. Bourg and A. M. Lubers, *Chem. Soc. Rev.*, 2009, **38**, 226–252.
10 F. Y. Cheng, J. Liang, Z. L. Tao and J. Chen, *Adv. Mater.*, 2011, **23**, 1695–1715.
11 C. J. Niu, J. S. Meng, X. P. Wang, C. H. Han, M. Y. Yan, K. N. Zhao, X. M. Xu, W. H. Ren, Y. L. Zhao, L. Xu, Q. J. Zhang, D. Y. Zhao and L. Q. Mai, *Nat. Commun.*, 2015, **6**, 7402.
12 Y. Zhao and L. Jiang, *Adv. Mater.*, 2009, **21**, 3621–3638.
13 G. Z. Fang, J. Zhou, Y. Hu, X. X. Gao, Y. Tang and S. Q. Liang, *J. Power Sources*, 2015, **275**, 694–701.
14 Q. Y. An, P. F. Zhang, Q. L. Wei, L. He, F. Y. Xiong, J. Z. Sheng, Q. Q. Wang and L. Q. Mai, *J. Mater. Chem. A*, 2014, **2**, 3297.
15 Y. H. Wang, Y. H. Wang, D. S. Jia, Z. Peng, Y. Y. Xia and G. F. Zheng, *Nano Lett.*, 2014, **14**, 1080–1084.
16 S. Luo, K. Wang, J. P. Wang, K. L. Jiang, Q. Q. Li and S. S. Fan, *Adv. Mater.*, 2012, **24**, 2294–2298.
17 C. B. Zhu, Y. Yu, L. Gu, K. Weichert and J. Maier, *Angew. Chem., Int. Ed.*, 2011, **50**, 6278–6282.
18 W. C. Duan, Z. Q. Zhu, H. Li, Z. Hu, K. Zhang, F. Y. Cheng and J. Chen, *J. Mater. Chem. A*, 2014, **2**, 8668.
19 X. P. Wang, C. J. Niu, J. S. Meng, P. Hu, X. M. Xu, X. J. Wei, L. Zhou, K. N. Zhao, W. Luo, M. Y. Yan and L. Q. Mai, *Adv. Energy Mater.*, 2015, **5**, 1500716.
20 N. Yabuuchi, M. Kajiyama, J. Iwatate, H. Nishikawa, S. Hitomi, R. Okuyama, R. Usui, Y. Yamada and S. Komaba, *Nat. Mater.*, 2012, **11**, 512–517.
21 X. H. Rui, W. P. Sun, C. Wu, Y. Yu and Q. Y. Yan, *Adv. Mater.*, 2015, **27**, 6670–6676.
22 G. Singh, J. M. L. del Amo, M. Galceran, S. Pérez-Villar and T. Rojo, *J. Mater. Chem. A*, 2015, **3**, 6954–6961.
23 Y. N. Zhou, J. Ma, E. Hu, X. Yu, L. Gu, K. W. Nam, L. Chen, Z. Wang and X. Q. Yang, *Nat. Commun.*, 2014, **5**, 5381.
24 J. Lee, A. Urban, X. Li, D. Su, G. Hautier and G. Ceder, *Science*, 2014, **343**, 519–522.
25 R. Baddour-Hadjean, A. Boudaoud, S. Bach, N. Emery and J. P. Pereira-Ramos, *Inorg. Chem.*, 2014, **53**, 1764–1772.
26 H. M. Liu, Y. G. Wang, L. Li, K. X. Wang, E. Hosono and H. S. Zhou, *J. Mater. Chem.*, 2009, **19**, 7885–7891.
27 S. Bach, A. Boudaoud, N. Emery, R. Baddour-Hadjean and J. P. Pereira-Ramos, *Electrochim. Acta*, 2014, **119**, 38–42.
28 W. Hu, X. B. Zhang, Y. L. Cheng, Y. M. Wu and L. M. Wang, *Chem. Commun.*, 2011, **47**, 5250–5252.
29 S. Yuan, Y. B. Liu, D. Xu, D. L. Ma, S. Wang, X. H. Yang, Z. Y. Cao and X. B. Zhang, *Adv. Sci.*, 2015, **2**, 1400018.
30 E. Uchaker and G. Z. Cao, *Chem.–Asian J.*, 2015, **10**, 1608–1617.
31 W. Hu, X. B. Zhang, Y. L. Cheng, C. Y. Wu, F. Cao and L. M. Wang, *ChemSusChem*, 2011, **4**, 1091–1094.
32 Y. F. Dong, S. Li, K. N. Zhao, C. H. Han, W. Chen, B. L. Wang, L. Wang, B. A. Xu, Q. L. Wei, L. Zhang, X. Xu and L. Q. Mai, *Energy Environ. Sci.*, 2015, **8**, 1267–1275.

33 Y. L. Zhao, C. H. Han, J. W. Yang, J. Su, X. M. Xu, S. Li, L. Xu, R. P. Fang, H. Jiang, X. D. Zou, B. Song, L. Q. Mai and Q. J. Zhang, *Nano Lett.*, 2015, **15**, 2180–2185.
34 Q. Y. An, J. Z. Sheng, X. Xu, Q. L. Wei, Y. Q. Zhu, C. H. Han, C. J. Niu and L. Q. Mai, *New J. Chem.*, 2014, **38**, 2075–2080.
35 Y. L. Cheah, N. Gupta, S. S. Pramana, V. Aravindan, G. Wee and M. Srinivasan, *J. Power Sources*, 2011, **196**, 6465–6472.
36 Z. L. Wang, D. Xu, L. M. Wang and X. B. Zhang, *ChemPlusChem*, 2012, **77**, 124–128.
37 H. G. Wang, D. L. Ma, Y. Huang and X. B. Zhang, *Chem.–Eur. J.*, 2012, **18**, 8987–8993.
38 L. Q. Mai, L. Xu, C. H. Han, X. Xu, Y. Z. Luo, S. Y. Zhao and Y. L. Zhao, *Nano Lett.*, 2010, **10**, 4750–4755.
39 D. W. Su and G. X. Wang, *ACS Nano*, 2013, **7**, 11218–11226.
40 Y. F. Dong, X. M. Xu, S. Li, C. H. Han, K. N. Zhao, L. Zhang, C. J. Niu, Z. Huang and L. Q. Mai, *Nano Energy*, 2015, **15**, 145–152.